Applied Physics Letters ARTICLE scitation.org/journal/apl

# Controlled rotation of micro-objects using acoustically driven microbubbles

Cite as: Appl. Phys. Lett. **118**, 063701 (2021); doi: 10.1063/5.0038789
Submitted: 26 November 2020 · Accepted: 29 January 2021 ·
Published Online: 11 February 2021



Yuyang Li,[1] Xiaoming Liu,[1,a)] Qiang Huang,[1] and Tatsuo Arai[1,2]

## AFFILIATIONS

[1]Key Laboratory of Biomimetic Robots and Systems, Ministry of Education, State Key Laboratory of Intelligent Control and Decision of Complex System, Beijing Advanced Innovation Center for Intelligent Robots and Systems, and School of Mechatronical Engineering, Beijing Institute of Technology, Beijing 100081, China
[2] Department of Mechanical and Intelligent Systems Engineering, The University of Electro-Communications, Tokyo 182-8585, Japan

[a)]Author to whom correspondence should be addressed: liuxiaoming555@bit.edu.cn

## ABSTRACT

Micromanipulation has significantly advanced both biomedical and industrial fields. However, there is still an urgent demand for controlled rotational manipulation at the microscale. Here, we report a noncontact rotational micromanipulation method using the acoustically driven microbubble contained in a micropipette. Acoustic vibration of the microbubble close to its resonant frequency was used to generate radiation force and microstreaming in the aqueous medium, allowing for trapping and rotating the micro-object. Simulation and particle visualization of the flow field clearly showed the microstreaming pattern induced by the oscillating microbubble. Experiments with different microbeads demonstrated the highly stable immobilization and rotation that related to the size and density of the microbead. By adjusting the frequency and voltage of the sinusoidal wave applied to the piezoelectric transducer, we demonstrated that the rotation frequency could be controlled over a broad range.



Over the last two decades, micromanipulation has significantly contributed to many biological and industrial fields including single-cell analysis,[1] cloning,[2] gene editing,[3] tissue engineering,[4] and testing and assembly of micro-optical/electronic components.[5] Controlled rotational micromanipulation has become essential, especially in stereoscopic examination, egg cell injection, and complex 3D assembly with attitude adjustment.[6–10] However, most traditional micromanipulation methods were developed for translational operations. Few of them are capable of controlled rotational operation with high accuracy, a broad velocity range, continuous 360° motion, and strong positional stability.

There are two main types of micromanipulation: contact and contactless. Industry widely uses micromanipulation based on direct physical contact and precise motorized micromanipulators.[11] However, continuous 360° rotation is still quite challenging for contact manipulation, and physical contact is harmful to cells and other valuable biological samples. Contactless micromanipulation using rotating optical,[12] electric,[13] and magnetic[14] fields or relative multiple position control makes remote rotational operation possible. However, the high laser intensity required in optical tweezers, heat induced by the electric current, and tagging of the targets by the external magnetic material make the biological targets susceptible to damage. Recently, on-chip acoustic–fluidic hybrid operation has emerged as a promising alternative micromanipulation technique with the appeal of strong force at low incident power, deep penetration into fluids, multiple functions including rotational operation, and excellent biocompatibility.[15–19] However, its functions and target sizes highly depend on the geometry of the microfluidic devices, whose predesigned structures and enclosed environment significantly limit flexibility in target selection. Thus, developing an acoustic–fluidic hybrid micromanipulation method to control rotation in an open environment can potentially solve these problems.

Here, we present a rotational manipulation method using an oscillating microbubble confined inside a microtubule that employs the dual effects of generated microstreaming and near-field radiation force to trap and rotate the micro-objects. The all-acoustic stimulation allows external macroscopic energy to accumulate and be released to the same dominant length scale as micro-objects. We utilize a low-power acoustic field to oscillate the microbubble confined inside a micropipette. When the frequency of the acoustic wave is close to the

resonant frequency of the microbubble, the remarkable reciprocating motion of the gas–liquid interface can drive the liquid to flow in and out of the micropipette and generate microstreaming nearby the orifice. The near-field radiation force and microstreaming generated by the oscillating microbubble enable immobilization and rotation of the micro-object. The wide range of rotation velocities controlled by the frequency and amplitude of the acoustic wave allows versatile applications, including 3D observation for low-speed requirements and efficient assembly at high speeds. Furthermore, the unenclosed environment permits complete access to specimens, which significantly facilitates full 3D operation and extended applications.

The experiments were conducted under a pair of orthogonally placed optical microscopes (Hirox, CX-10C), as shown in Fig. 1(a). To generate a position-controlled microbubble, we chose a micropipette (inner and outer diameters of 180 $\mu$m and 250 $\mu$m, respectively) filled with a certain amount of solidified polydimethylsiloxane to form a cavity at its orifice. As the cavity was submerged in the liquid of the glass dish, a cylindrical bubble formed inside under surface tension. The bubble was carried as an operating terminal by the micropipette and placed on a positioning stage, allowing efficient and flexible handling of various complex tasks. A piezoelectric transducer was epoxy glued to the bottom of the glass dish adjacent to the center of operation to emit acoustic waves driven by a function generator (GW Instek, AFG-2225).

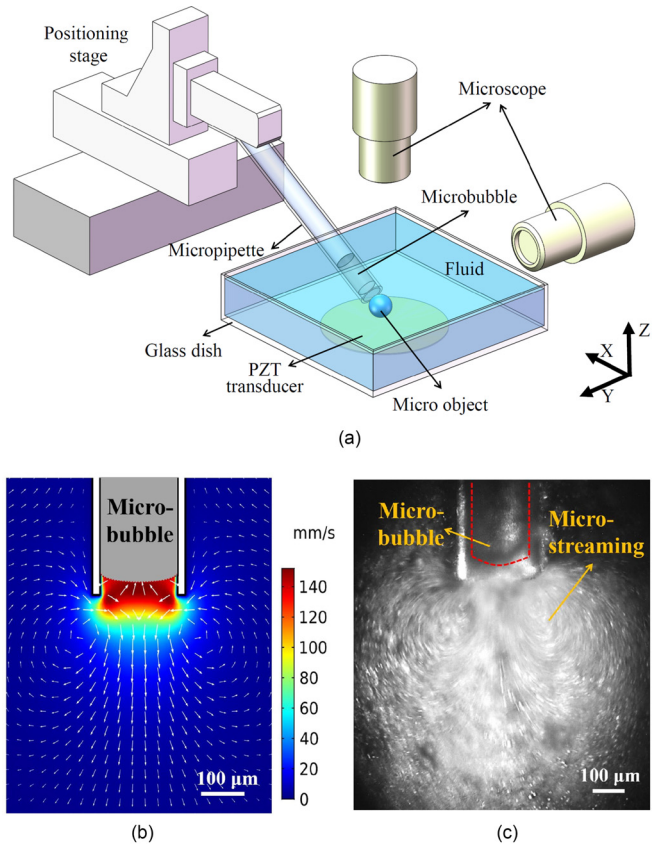


**FIG. 1.** (a) Experimental setup for noncontact manipulation using an acoustically driven microbubble. (b) 2D slice plots of the microstreaming field around the microbubble using COMSOL Multiphysics. (c) Optical image of acoustic microstreaming during microbubble oscillation at a driving frequency of 5.6 kHz and a peak voltage of 15 V.

Large differences in the physical states of the gas and liquid phases contribute to the sensitivity and specificity of the bubbles in the acoustic field. In an unbounded Newtonian fluid, a captured microbubble oscillates periodically under the surrounding acoustic pressure when it is exposed to an acoustic field with a wavelength much larger than its diameter. The maximum amplitude occurs when the frequency of the acoustic wave approaches the resonant frequency of the microbubble.[20] For a bubble in a tube, the resonant frequency is estimated as[21]

$$f_0 \approx \frac{1}{2\pi}\sqrt{\frac{3\pi\kappa P_0}{8RL\rho}}, \tag{1}$$

where $\kappa$ is the adiabatic index (1.4 for air); $P_0$ is the atmospheric pressure; $R$ and $L$ are the diameter and length of the cylindrical bubble, respectively; and $\rho$ is the density of the liquid outside the bubble. For sub-millimeter microbubbles, the resonant frequency is typically above the kHz level. Such high-frequency oscillations of the gas–liquid interface contribute to regular time-averaged streaming around the micropipette orifice, which can be utilized for micromanipulation.[22,23]

To obtain pronounced microstreaming, the drive frequency is set at the resonance value predicted using Eq. (1). Figures 1(b) and 1(c) show the simulation and experimental results, respectively, for the microbubble oscillating at its resonant frequency of 5.6 kHz at the peak voltage of 15 V of the driven sinusoidal signal (see Video S1 in the supplementary material). Under this condition, regularly and symmetrically distributed vortices with flow velocities exceeding 100 mm/s are generated, which vary regularly according to the acoustic waves with different amplitudes and frequencies. This result implies that the rotation could be controlled by adjusting the amplitudes and frequencies of the acoustic waves to affect the generated microstreaming. Additionally, in the experiments, the microbubble was completely recessed into the micropipette since the liquid in the glass dish flowed into the micropipette and submerged part of the cavity under the influence of surface tension. The microbubble kept a proper distance from the micropipette orifice to avoid the influence of the convex gas–liquid interface on the distribution of the generated microstreaming and decay of the near-field radiation force from the oscillating microbubble.

In addition to the apparent microflow generation, the oscillating microbubbles scatter part of the energy absorbed by the incident acoustic waves into the surrounding environment. Objects in their vicinity, whether soft or rigid, undergo a change in momentum due to the pressure gradient. This is an effect of the secondary radiation force[24] or Bjerknes force,[25]

$$F_{Radiation} = 4\pi\rho\frac{\rho-\rho_p}{\rho+2\rho_p}\frac{R^4R_p^3}{d^5}\omega^2\varepsilon^2, \tag{2}$$

where $\rho_p$ and $R_p$ are the density and radius of the microbead, respectively; $d$ refers to the distance between the bubble and the center of the microbead; and $\omega$ and $\varepsilon$ refer to the angular frequency and amplitude of the oscillating microbubble, respectively. This formula shows that

the secondary radiation force is a near-field force that depends highly on the distance between the object and the bubble. The direction of this force is determined by the density of the liquid and the target object. For common micro-objects sunk at the bottom of the liquid, the secondary radiation force received is directed toward the oscillating bubble.

As the micropipette approaches, the microbead can be trapped and immobilized nearby with the predominant contribution of attractive radiation force. For a polystyrene (PS) bead (density $1.05 \times 10^3$ kg/m$^3$) in Fig. 2, diameter 160 $\mu$m, rotating at a drive frequency of 5.5 kHz, using Eq. (2), the secondary radiation force can be estimated as $F_{Radiation} \approx 3.48$ nN, and the remaining gravity offsetting buoyancy is $G_r = (4/3)\pi R^3(\rho_p - \rho)g = 1.05$ nN. Due to the state of force equilibrium, the streaming force on the microbead can be estimated as $F_{streaming} = \left|\vec{F}_{Radiation} - \vec{G}_r\right| \approx 2.83$ nN. Using the amplitude or frequency of the acoustic wave to tune the oscillation intensity of the microbubble in a small range alters both the radiation and streaming forces, causing the microbead to be in equilibrium soon at another position. Generally, during the initial trapping process, the microbead most possibly stabilizes at the low half of the vortex as it moves upward to approach the micropipette. Then, the streaming above the microbead with higher velocity than the streaming below from the micropipette becomes the dominant force driving the microbead to rotate in the counterclockwise direction. This has been confirmed in our extensive experiments, as shown in Fig. 2 (also see Video S2 in the supplementary material). The angular speed $\Omega$ suggests that the driving streaming torque $T_{streaming}$ on the microbead is balanced by the drag torque $T_D = 8\pi\mu R_p^3\Omega = 0.53$ pN·m from the surrounding water with viscosity $\mu = 1.01$ mPa s. During rotating, the microbead experiences only microscopic forces provided by the oscillating microbubble and streaming around in addition to gravity and buoyancy. This noncontact state avoids the possible perturbation caused by direct physical contact, which is important for the noninvasive manipulation of biological objects at the microscale. Once the microbubble stops oscillating, the microbead stops experiencing radiation and streaming forces and will immediately stop rotating due to the low Reynolds number approximation $\mathrm{Re} = R_p^2\omega/\mu \ll 1$ at the microscale and then sinks to the bottom.

The amplitude and frequency of the acoustic wave are adjustable parameters for rotation; therefore, other conditions are held invariant to quantify the relationship between these two parameters and the rotation frequency. The square glass dish used in the experiment had dimensions of $80 \times 80 \times 15$ mm$^3$, and the liquid inside was deionized water with a height of 10 mm, at the bottom of which were deposited microbeads with a diameter of 160 $\mu$m. A sinusoidal signal with a constant peak voltage of 5 V was applied to the terminal of the piezoelectric transducer, the frequency of which varied from 3 kHz to 8 kHz, and a set of data was recorded at 0.1 kHz intervals. This process was recorded by a high-speed camera to calculate the rotation frequency of the microbead driven by the corresponding acoustic frequencies. Figure 3(a) shows the result corresponding to the fastest rotation frequency around the resonant frequency of the microbubble. The same method was used to obtain the effect of the input voltage on microbead rotation frequency as shown in Fig. 3(b). The equilibrium was easily broken when the input voltage exceeded a high or low threshold (>25 V or <3 V in this experiment) and the rotation terminated. When the input voltage was above 25 V, the microbead was "blown" out by a violent flow field, and when the input voltage was below 3 V, gravity prevailed.

To analyze the physical properties of the microbeads that could affect the rotation, microbeads made of PS, polymethyl methacrylate (PMMA, density $1.2 \times 10^3$ kg/m$^3$), and glass (density $2.5 \times 10^3$ kg/m$^3$) in different sizes were selected as the experimental objects. As shown in Fig. 3(b), the increase in diameter significantly reduces the rotation frequency. We also found that for a given size of the micropipette, a microbead that is too large (over 200 $\mu$m here) cannot be rotated or

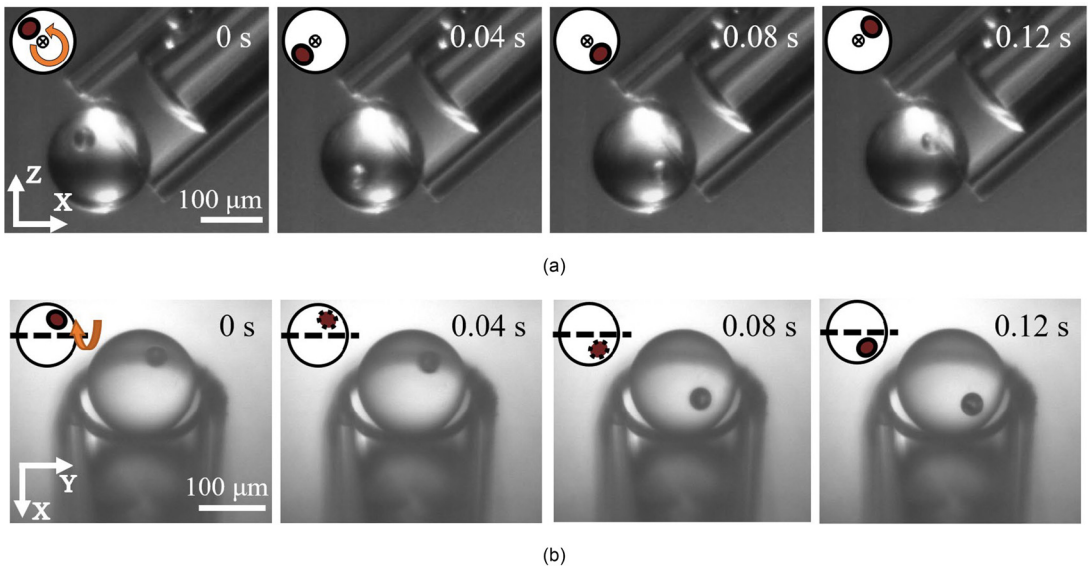


**FIG. 2.** Sequence of time-stamped optical images of the rotation of a black dot-marked microbead at a driving frequency of 5.5 kHz and a peak voltage of 10 V. (a) Side view in the X–Z plane. (b). Top view in the X–Y plane.

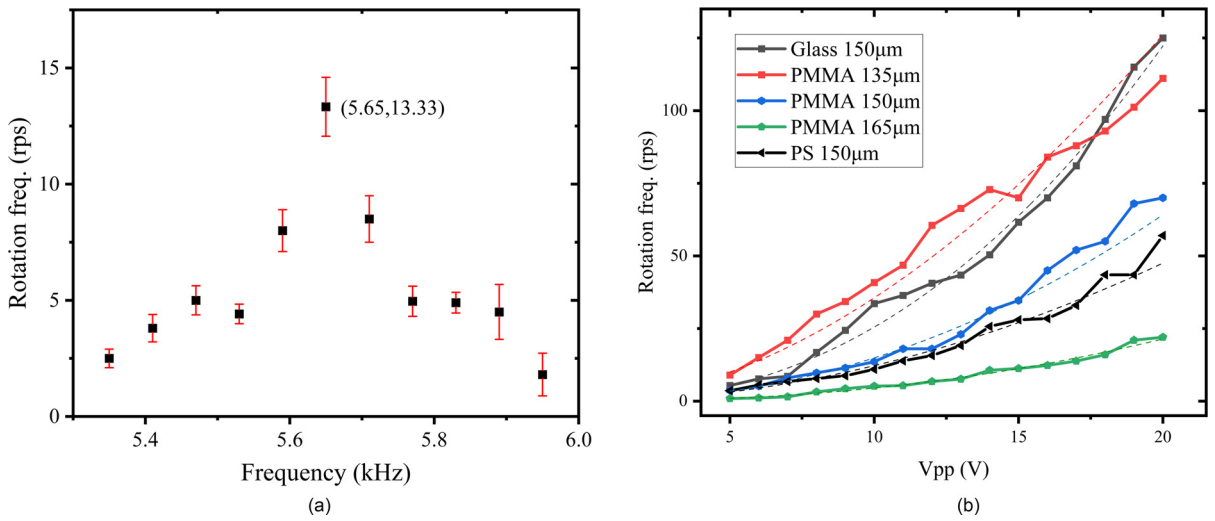


**FIG. 3.** (a) Dependence of the microbead's rotation frequency on the acoustic frequency when the input voltage peak is constant at 5 V. We see a noticeable peak at frequencies between 5.6 and 5.7 kHz. (b) Plot of rotation frequency against driving voltage Vpp of different densities and sizes of microbeads with a constant excitation frequency of 5.5 kHz; their exponential fitting factors are 2.26 for glass—150 $\mu$m, 1.83 for PMMA—135 $\mu$m, 2.15 for PMMA—150 $\mu$m, 2.24 for PMMA—165 $\mu$m, and 1.85 for PS—150 $\mu$m, respectively.

even captured due to insufficient driving force. Also, changes in density significantly affect $G_r$ and $F_{Radiation}$. In this experiment, the resultant forces of $G_r$ and $F_{Radiation}$ on PS, PMMA, and glass beads with a 150 $\mu$m diameter are 2.50 nN, 8.98 nN, and 34.1 nN, respectively. With the same driving conditions, the greater $\left|\vec{F}_{Radiation} - \vec{G}_r\right|$ drives the microbead to move closer to the orifice and axis of the micropipette and is balanced by the increased streaming force due to higher streaming velocity. Accordingly, a higher rotation frequency can also be achieved. However, excessive density can lead to an absolute dominance of remaining gravity, making it difficult to be picked up. In addition, we present the exponential relationship between rotation frequency and voltage. The microstreaming velocity $u$ due to an oscillating bubble is given by $u = \frac{R^4}{d^5}\omega\varepsilon^2$.[26] Owing to the positive correlation between the driving voltage and the microbubble amplitude,[27] the experimentally obtained exponential fitting factors are 2.26, 1.83, 2.15, 2.24, and 1.85, respectively, agreeing well with the theory. The slight deviation from a precise quadratic relationship is not surprising, considering that the spatial position of the microbead can change slightly and the acoustic microstreaming is complex in the vicinity.

The fluctuation in spatial position of the target object during rotation is an important measure of the method. This directly affects 3D reconstruction accuracy, single-cell analysis, and other applications requiring high positional stability. Thus, we held all experimental conditions constant and observed simultaneously from the side and top. We calculated the spatial position offset of the rotating beads using a computer-aided vision system, as shown in Fig. 4. The results show that the position fluctuations of the rotating microbead along the X, Y, and Z axes were all less than 4 $\mu$m over 9 min, which is sufficient for most micromanipulations. Normally, in the absence of large external vibrational perturbations, the microbead does not fluctuate significantly (less than 3 $\mu$m). Over time, the intensely oscillating microbubble can shift the position of the gas–liquid interface away from its initial state, thus altering the microstreaming to shift the position of the microbead.

In summary, our proposed oscillating microbubbles driven by acoustic waves can be used to control rotation. The physical mechanisms behind this accessible and effective device have been clarified by theoretical and quantitative analysis of the forces and torque acting on the objects. Rotation frequency related to the acoustic parameters and microbead properties has been studied experimentally. In addition, the maximum position fluctuations of the PS microbead during rotation less than 4 $\mu$m indicated high positional stability of the proposed method, which can significantly contribute to the 3D observation at

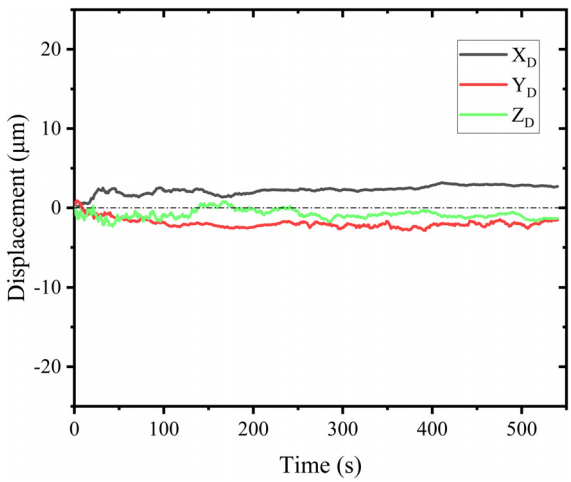


**FIG. 4.** Position fluctuation during rotation of a PS microbead with a diameter of 160 $\mu$m at a driving frequency of 5.5 kHz and a peak voltage of 10 V. Black, red, and blue curves denote the fluctuations in the X, Y, and Z directions, respectively.

the microscale. With its simplicity, noncontact, controllability, and stability, this strategy can significantly expedite the use of micromanipulation in biology and industry. We now aim to expand the range of target object sizes and flexible omnidirectional control to broaden its application and perform diverse biocompatibility tests.

See the supplementary material for (1) the acoustic microstreaming around an oscillating microbubble (Video S1) and (2) the acoustic induced rotation of a marked microbead (Video S2).

This work was supported by the National Natural Science Foundation of China (Grant Nos. 61873037 and 61903039); the China Postdoctoral Science Foundation (Nos. BX20190035 and 2020M680015); and a Grant-in-Aid for Scientific Research (No. 19H02093) from the Ministry of Education, Culture, Sports, Science and Technology of Japan.

## DATA AVAILABILITY

The data that support the findings of this study are available from the corresponding author upon reasonable request.

## REFERENCES

[1]S. Lindström and H. Andersson-Svahn, Lab Chip **10**, 3363 (2010).
[2]A. G. Fraser, R. S. Kamath, P. Zipperlen, M. Martinez-Campos, M. Sohrmann, and J. Ahringer, Nature **408**, 325 (2000).
[3]R. W. Carlsen and M. Sitti, Small **10**, 3831 (2014).
[4]X. Liu, Q. Shi, H. Wang, T. Sun, N. Yu, Q. Huang, and T. Fukuda, IEEE/ASME Trans. Mechatronics **23**, 667 (2018).
[5]K. Tsui, A. A. Geisberger, M. Ellis, and G. D. Skidmore, J. Micromech. Microeng. **14**, 542 (2004).
[6]X. Liu, Q. Shi, Y. Lin, M. Kojima, Y. Mae, T. Fukuda, Q. Huang, and T. Arai, Small **15**, e1804421 (2019).
[7]A. Barbot, M. Power, F. Seichepine, and G.-Z. Yang, Sci. Adv. **6**, eaba5660 (2020).
[8]L. Feng, P. Di, and F. Arai, Int. J. Rob. Res. **35**, 1445 (2016).
[9]X. Wang, C. Ho, Y. Tsatskis, J. Law, Z. Zhang, M. Zhu, C. Dai, F. Wang, M. Tan, S. Hopyan, H. McNeill, and Y. Sun, Sci. Robot. **4**, eaav6180 (2019).
[10]D. Baresch, J. L. Thomas, and R. Marchiano, Phys. Rev. Lett. **121**, 074301 (2018).
[11]M. Power, A. J. Thompson, S. Anastasova, and G. Z. Yang, Small **14**, e1703964 (2018).
[12]W. Hu, K. S. Ishii, and A. T. Ohta, Appl. Phys. Lett. **99**, 094103 (2011).
[13]Y. T. Chow, T. Man, G. F. Acosta-Vélez, X. Zhu, X. Wen, P. S. Chung, T. "Leo" Liu, B. M. Wu, and P. Y. Chiou, Adv. Sci. **5**, 1700711 (2018).
[14]C. Gosse and V. Croquette, Biophys. J. **82**, 3314 (2002).
[15]M. Hagiwara, T. Kawahara, and F. Arai, Appl. Phys. Lett. **101**, 074102 (2012).
[16]P. Zhang, C. Chen, F. Guo, J. Philippe, Y. Gu, Z. Tian, H. Bachman, L. Ren, S. Yang, Z. Zhong, P. H. Huang, N. Katsanis, K. Chakrabarty, and T. J. Huang, Lab Chip **19**, 3397 (2019).
[17]L. Feng, B. Song, Y. Chen, S. Liang, Y. Dai, Q. Zhou, D. Chen, X. Bai, Y. Feng, Y. Jiang, D. Zhang, and F. Arai, Biomicrofluidics **13**, 64103 (2019).
[18]A. Ozcelik, N. Nama, P. H. Huang, M. Kaynak, M. R. McReynolds, W. Hanna-Rose, and T. J. Huang, Small **12**, 5120 (2016).
[19]V. H. Lieu, T. A. House, and D. T. Schwartz, Anal. Chem. **84**, 1963 (2012).
[20]T. G. Leighton and R. E. Apfel, J. Acoust. Soc. Am. **96**, 2616 (1994).
[21]T. Qiu, S. Palagi, A. G. Mark, K. Melde, F. Adams, and P. Fischer, Appl. Phys. Lett. **109**, 191602 (2016).
[22]S. A. Elder, J. Acoust. Soc. Am. **31**, 54 (1959).
[23]P. Marmottant and S. Hilgenfeldt, Nature **423**, 153 (2003).
[24]W. L. Nyborg, J. Acoust. Soc. Am. **42**, 947 (1967).
[25]V. Bjerknes, *Fields of Force: Supplementary Lectures, Applications to Meteorology; A Course of Lectures in Mathematical Physics Delivered December 1 to 23, 1905* (The Columbia University Press, 1906).
[26]D. L. Miller, J. Acoust. Soc. Am. **84**, 1378 (1988).
[27]D. Ahmed, M. Lu, A. Nourhani, P. E. Lammert, Z. Stratton, H. S. Muddana, V. H. Crespi, and T. J. Huang, Sci. Rep. **5**, 9744 (2015).